

DISCOVERY OF A NEW PULSAR WIND NEBULA IN THE LARGE MAGELLANIC CLOUD

B. M. GAENSLER¹, S. P. HENDRICK², S. P. REYNOLDS^{1,2} AND K. J. BORKOWSKI²

Draft version May 22, 2019

ABSTRACT

We present new high-resolution radio and X-ray observations of the supernova remnant (SNR) B0453–685 in the Large Magellanic Cloud, carried out with the Australia Telescope Compact Array and the *Chandra X-ray Observatory* respectively. Embedded in the SNR shell is a compact central nebula producing both flat-spectrum polarized radio emission and non-thermal X-rays; we identify this source as a pulsar wind nebula (PWN) powered by the relativistic wind of an unseen central neutron star. We present a new approach by which the properties of a SNR and PWN can be used to infer upper limits on the initial spin period and surface magnetic field of the unseen pulsar, and conclude that this star was an initial rapid rotator with current properties similar to those of the Vela pulsar. As is the case for other similarly-aged sources, there is currently an interaction taking place between the PWN and the SNR’s reverse shock.

Subject headings: ISM: individual (B0453–685) — stars: neutron — supernova remnants — Magellanic Clouds — radio continuum: ISM — X-rays: ISM

1. INTRODUCTION

The Magellanic Clouds are ideal regions for studying supernova remnants (SNRs) and their environments, the known distance and low extinction obviating many of the frustrations associated with studying Galactic SNRs. While this has proved very useful in studying the shell emission produced by the interaction of SNRs with the interstellar medium, just two Magellanic Systems, SNRs B0540–693 (Manchester, Staveley-Smith, & Kesteven 1993) and N 157B (Wang et al. 2001), are known to harbor a young energetic pulsar and its surrounding pulsar wind nebula (PWN). The lack of other PWNe in the Magellanic Clouds is most likely due to a lack of spatial resolution — such resolution is only now being applied to Magellanic SNRs in both the radio and X-ray bands, and so the prospects are good for identifying new “composite” SNRs, containing both outer shells and central PWNe. Such sources are of particular interest, as the shell and PWN together provide unique constraints on the properties of the system.

We here present the identification of one such composite SNR, B0453–685 in the Large Magellanic Cloud (LMC). This *Letter* primarily discusses radio and X-ray observations of the central PWN. Interpretation of the surrounding shell will be the focus of a subsequent paper (Hendrick et al. 2003).

2. OBSERVATIONS AND RESULTS

Radio observations of B0453–685 were carried out with the Australia Telescope Compact Array (ATCA). Observations were made simultaneously at 1.4 and 2.4 GHz with a bandwidth of 128 MHz at each frequency, using the 1.5G³ and 6.0C array configurations on 2002 Jul 23 and 2002 Aug 26 respectively. An X-ray observation of the same field of duration 38.6 ks was carried out using the ACIS-S3 detector of the *Chandra X-ray Observatory* on 2001 Dec 18.

For each radio observation, the time on source was approximately 11 hr. Antenna gains and polarization leakages were calibrated using regular observations of PKS B0252–712, while

the flux density scale was set by observations of PKS B1934–638. The radio data were edited, calibrated and imaged using standard techniques,⁴ the resulting resolution at each frequency is listed in Table 1. Analysis of the *Chandra* data will be reported in detail elsewhere (Hendrick et al. 2003).

2.1. Imaging and Polarimetry

Radio and X-ray images of SNR B0453–685 are shown in Figure 1. At radio frequencies, the source is clearly resolved into two components: a bright central core, embedded in an approximately circular limb-brightened shell. Table 1 lists the flux densities of these two components at 1.4 and 2.4 GHz after applying a correction for the local background. Fitting an ellipse to the perimeter of the shell component, we find that if one excludes the bright protrusion to the southwest, the shell can be fitted by a circle of diameter $120'' \pm 4''$, centered at RA (J2000) $04^{\text{h}}53^{\text{m}}37\text{.}2$, Decl. (J2000) $-68^{\circ}29'30''$ (with an approximate uncertainty of $\pm 2''$). For a distance $50d_0$ kpc, the diameter of the shell is $(29 \pm 1)d_0$ pc.

As can be seen in Figure 2, the central radio core is elongated along a position angle of $\sim 45^\circ$, with approximate dimensions $30'' \times 20''$ corresponding to a spatial size of $7.3d_0$ pc $\times 4.8d_0$ pc. The core is brightest at its north-eastern extent, where it is dominated by an approximately circular, slightly extended region of emission, with peak position RA (J2000) $04^{\text{h}}53^{\text{m}}38\text{.}6$, Dec. (J2000) $-68^{\circ}29'21\text{.}7''$ (with an uncertainty of $\pm 0\text{.}5''$ in each coordinate). This region also shows significant linear polarization, of mean fractional intensity 6% at 1.4 GHz and 8% at 2.4 GHz, as shown in Figure 2. The brightest region of the core is offset from the center of the shell by $11'' \pm 2''$. To the south-west, the surface brightness of the core steadily fades with increasing distance from the brightest region.

As can be seen in the lower-left panel of Figure 1, the morphology of B0453–685 in the soft X-ray band shows a broadly similar structure to that seen in the radio, again revealing a central core surrounded by a limb-brightened shell. In the hard X-

¹Harvard-Smithsonian Center for Astrophysics, 60 Garden Street MS-6, Cambridge, MA 02138; bgaensler@cfa.harvard.edu

²Department of Physics, North Carolina State University, Raleigh, NC 27695

³1.5G is a non-standard ATCA configuration, and has successive spacings between the six antennas of 30.6, 535.7, 306.1, 413.3 and 3015.3 meters.

⁴See <http://www.atnf.csiro.au/computing/software/miriad>.

ray band (lower-right panel of Figure 1), only the central core is visible. The extent of this region is $14'' \times 7''$ ($3.4d_0$ pc \times $1.7d_0$ pc), less than half that seen in the radio. Figure 2 demonstrates that the positions of the peak emission in the X-ray and radio cores coincide to within the resolution of the observations.

2.2. Spectral Analysis

We have carried out a spectral index study of the radio data by smoothing the 1.4 and 2.4 GHz images to a common resolution of $15''$ and then applying spectral tomography to the resulting maps (Katz-Stone & Rudnick 1997). This analysis demonstrates that the central core has a distinctly flatter radio spectrum than the surrounding shell: we determine a spectral index $\alpha = -0.10 \pm 0.05$ for the core and $\alpha = -0.5 \pm 0.1$ for the shell ($S_\nu \propto \nu^\alpha$). Assuming a constant spectrum $\alpha = -0.10$ for the core between 10^7 and 10^{11} Hz, the radio luminosity of this component is $L_R \sim 2d_0^2 \times 10^{34}$ erg s $^{-1}$.

At X-ray energies, we have determined the spectral properties of the different components of the SNR by extracting events from appropriate source and background regions and fitting to the resulting spectra, as will be described in detail by Hendrick et al. (2003). To briefly summarize their results, the shell component is well-fitted by a Sedov model with foreground absorption, while the central core can be fit by an absorbed power law. The best-fit parameters for the core are a foreground absorbing column $N_H = (1.3 \pm 0.2) \times 10^{21}$ cm $^{-2}$, a spectral index $\alpha = -0.9 \pm 0.4$ and an unabsorbed flux density at 1 keV $f_X = (6 \pm 1) \times 10^{-14}$ erg cm $^{-2}$ s $^{-1}$ keV $^{-1}$ (uncertainties quoted at 90% confidence). The corresponding X-ray luminosity over the energy range 0.5–10 keV is $L_X \sim 6d_0^2 \times 10^{34}$ erg s $^{-1}$. The spectral fits for the surrounding shell imply an age $\tau \approx 13$ kyr, a swept-up mass $M_{sw} \approx 280M_\odot$, an upstream density $n_0 \approx 0.4$ cm $^{-3}$ and an initial explosion energy $E_0 \approx 5 \times 10^{50}$ ergs.

3. DISCUSSION

The core seen embedded in SNR B0453–685 is centrally located, has a filled-center morphology, has a flat spectrum and is linearly polarized at radio wavelengths, and is coincident with a smaller non-thermal X-ray nebula. All these properties demonstrate that B0453–685 is a composite SNR, containing a synchrotron-emitting PWN powered by a neutron star embedded in a shell SNR. This is only the third PWN identified in the Magellanic Clouds.

3.1. Properties of the Central Pulsar

Within the core, no point source corresponding to the central pulsar is apparent at either radio or X-ray wavelengths. We can calculate upper limits on the flux from such a source as follows. At radio wavelengths, we made images of the field using only the longest (> 3000 meters) five baselines in each configuration, so as to filter out most of the extended emission. At both 1.4 and 2.4 GHz, the brightest region of the core was still detected in these images. The corresponding upper limit on emission from a point source at the peak of nebular emission is 3 mJy and 0.4 mJy at 1.4 and 2.4 GHz, respectively.

In the X-ray band, we employed the SHERPA package⁵ to carry out two-dimensional fitting to the nebular morphology (e.g. Murray et al. 2002). We fit the core with three components: an elliptical gaussian to define the overall shape of the core, an unresolved source (with spatial extent corresponding to the point spread function of the telescope) centered on

the peak of the X-ray emission to represent the emission from an embedded point source, and a constant offset to account for background emission. Using these three components, we find that in the energy range 0.3–10 keV, the best-fit model contains 49 ± 26 counts in an unresolved central source (uncertainty quoted at 90% confidence). This suggests marginal evidence for a point source — in subsequent discussion we adopt 49 counts as an upper limit, corresponding to a count-rate $< 1.3 \times 10^{-3}$ cts sec $^{-1}$. Assuming a column density $N_H = 1.3 \times 10^{21}$ cm $^{-2}$ and a power law spectrum with a photon index $\Gamma = 1.5$ (typical for a young pulsar), this corresponds to an unabsorbed X-ray luminosity (0.5–10 keV) $L_X < 5d_0^2 \times 10^{33}$ ergs s $^{-1}$.

These radio and X-ray upper limits on unresolved emission from a central pulsar are not especially constraining. Our radio upper limit is insufficient to detect any but the most luminous radio pulsars known, and is more than an order of magnitude above the upper limit for radio pulsations at this position from the recent survey of Manchester et al. (2003). Several young pulsars have been recently identified with a point-source X-ray luminosity $L_X \approx 10^{32} - 10^{33}$ ergs s $^{-1}$ (Murray et al. 2002; Hughes et al. 2003), well below the upper limit seen here.

In the absence of any direct detection of emission, a first guess as to the properties of the central pulsar in B0453–685 can come from comparison with other similar systems. There are ~ 20 other shell SNRs known to contain a central X-ray/radio PWN (Kaspi & Helfand 2002). Of these other sources, the properties of SNR B0453–685 most closely resemble those of the Vela SNR and of SNR G0.9+0.1, as demonstrated in Table 2. The similarity of these three systems argues that SNR B0453–685 is most likely powered by a “Vela-like” pulsar (e.g. Kramer et al. 2003), with a spin-period $P \sim 100$ ms, a surface magnetic field $B \sim 3 \times 10^{12}$ G and a current spin-down luminosity $\dot{E} \approx 10^{37}$ ergs s $^{-1}$.

In the many cases in which a PWN has no identified pulsar, considerable further effort has been invested to infer the properties of the unseen central source (i.e. current spin period P , initial spin period P_0 , period derivative \dot{P} and surface magnetic field B) from those of its PWN. The age, spin-down luminosity and surface magnetic field of the system are, respectively (Manchester & Taylor 1977):

$$\tau = \frac{P}{(n-1)\dot{P}} \left[1 - \left(\frac{P_0}{P} \right)^{n-1} \right], \quad (1)$$

$$\dot{E} = 4\pi^2 I \frac{\dot{P}}{P^3}, \quad (2)$$

$$B = 3.2 \times 10^{19} (P\dot{P})^{1/2} \text{ G} \quad (3)$$

where $I \equiv 10^{45}$ g cm 2 is the neutron star moment of inertia, $n \equiv 2 - P\ddot{P}/\dot{P}^2$ is the pulsar’s “braking index”, and P is in seconds. Typically one assumes $n = 3$, $P_0 = 0$ and $L_X = \eta\dot{E}$ (where η is an assumed efficiency factor). The values of L_X and τ are determined from observations, from which one can then derive estimates for P , \dot{P} and B from the above equations.

Here we propose an alternative approach, where rather than assuming an (unphysical) value of P_0 , we use the above expressions to eliminate P and \dot{P} , and thus obtain a relation between B and P_0 . Assuming that B is constant with time, the resulting function has absolute maxima in both B and P_0 . The robust

⁵See http://cxc.harvard.edu/ciao/download/doc/sherpa_html_manual.

upper limits on the surface magnetic field and the initial spin period of the neutron star which result are:

$$B < 3.2 \times 10^{19} \frac{U}{\tau(n-1)} \text{ G}; \quad P_0 < U(\tau[n+1])^{-1/2} \left(\frac{2}{n+1} \right)^{\frac{1}{n-1}}, \quad (4)$$

where $U^2 = P^3/\dot{P} = 4\pi^2 I \eta / L_X$. These limits are reasonably insensitive to the exact value of n assumed; if we adopt $2 < n < 3$ (encompassing the observed range for the four pulsars for which n has been directly measured; e.g. Camilo et al. 2000; Cusumano, Massaro, & Mineo 2003), we find $B < (3.1 - 6.3)\eta^{1/2} \times 10^{13} \text{ G}$ and $P_0 < (448 - 488)\eta^{1/2} \text{ ms}$ for this system. Of other PWNe and their associated pulsars, a solid upper limit to the efficiency with which X-ray emission is produced is $\eta < 0.05$; we have argued above that the central pulsar here is a “Vela-like” pulsar, for which $\eta \approx 0.01 - 0.001$ is more reasonable (e.g. Possenti et al. 2002). We therefore conclude that the central neutron star in this system has a surface magnetic field $B < 6 \times 10^{12} \text{ G}$ and an initial spin period $P_0 < 50 \text{ ms}$. These values are consistent with a “typical” radio pulsar such as the Crab ($B = 4 \times 10^{12} \text{ G}$, $P_0 = 19 \text{ ms}$) and Vela ($B = 3 \times 10^{12} \text{ G}$) pulsars, but not with the emerging class of young pulsars which are highly magnetized and/or slow initial rotators, such as PSR J1846–0258 ($B = 5 \times 10^{13} \text{ G}$; Gotthelf et al. 2000) or PSR J1210–5226 ($P_0 \approx 400 \text{ ms}$; Pavlov et al. 2002).

3.2. Evolutionary State of the PWN

Chevalier (1998) divides the evolution of PWNe into successive phases. The PWN first expands supersonically into the low density interior of the SNR. At later stages, the PWN collides with the reverse shock of the SNR; this interaction can compress the pulsar nebula, and also causes it to expand more slowly. If the pulsar has sufficient space velocity its motion can later become supersonic in the shocked SNR interior, and it then drives a bow-shock PWN.

The morphology and size of the PWN seen here provides constraints on the evolutionary state of this system. If we assume that the pulsar spin-down luminosity is constant in the initial supersonically expanding phase, the radius of the PWN evolves such that $R_{\text{PWN}} = 0.839 \times (\dot{E}\tau/E_0)^{1/5} V_0 \tau$, where V_0 was the initial expansion velocity of the SNR shell (van der Swaluw et al. 2001). In this case we observe $R_{\text{PWN}} \approx 3 \text{ pc}$, $\tau \approx 13 \text{ kyr}$ and $E_0 \approx 5 \times 10^{50} \text{ ergs}$, and we adopt $\dot{E} = E_{37} \times 10^{37} \text{ ergs s}^{-1}$. Thus if the PWN is still in this first phase of evolution, we require $V_0 \approx 700 E_{37}^{-1/5} \text{ km s}^{-1}$, implying an enormous ejected mass $M_{ej} = 2E_0/V_0^2 \approx 100 E_{37}^{2/5} M_\odot$. We thus conclude that the PWN is almost certainly not expanding supersonically, having a radius much smaller than expected in this interpretation.

The brightest radio and X-ray emission from the PWN is offset from the SNR’s geometric center by $l = (2.7 \pm 0.5)d_0 \text{ pc}$. Since the peak of X-ray emission most likely marks the current position of the unseen pulsar, a possible interpretation is that the

pulsar is moving away from the presumed explosion site with a transverse velocity $V_T = l/\tau = 200 \pm 40 \text{ km s}^{-1}$, which is quite typical for a young pulsar. The radio PWN is clearly elongated, with a fading tail pointing back along the implied direction of motion. While this is suggestive of a bow shock morphology as seen around some high-velocity pulsars in SNRs (e.g. Frail et al. 1996), such a situation requires that the pulsar be moving supersonically through shocked ejecta. In the Sedov solution, this condition is met only when $l/R_{\text{SNR}} \gtrsim 0.7$ (van der Swaluw, Achterberg, & Gallant 1998). Unless the pulsar’s motion is at less than $\sim 20^\circ$ to the line-of-sight (implying a true space velocity $V > 700 \text{ km s}^{-1}$), the pulsar in this system is still too close to the center of its SNR to meet this requirement.

The only remaining possibility is that this PWN has undergone a reverse shock interaction with its surrounding SNR, and is now expanding subsonically. Such an interaction is expected to begin at an age $\sim 10 \text{ kyr}$ when the SNR has swept up $\gtrsim 10$ times its own mass (Chevalier 1998); these requirements are consistent with those seen for this source. The elongated morphology and comparatively small radius seen for the radio PWN are both simply accounted for by reverse-shock compression; the same properties have been similarly interpreted in both the other SNRs listed in Table 2 (Gaensler, Pivovaroff, & Garmire 2001; Blondin, Chevalier, & Frierson 2001).

4. CONCLUSIONS

New radio and X-ray observations of SNR B0453–685 in the LMC clearly demonstrate this source to be a composite SNR, consisting of both an outer shell and a central pulsar-powered nebula. We have used the properties of this source to infer that the unseen central neutron star is a typical young radio pulsar, with an initial spin period $P_0 < 50 \text{ ms}$, a current period $P \sim 100 \text{ ms}$, a surface magnetic field $B < 6 \times 10^{12} \text{ G}$, a spin-down luminosity $\dot{E} \sim 10^{37} \text{ erg s}^{-1}$ and a relatively low space velocity $V \sim 200 \text{ km s}^{-1}$. The small extent and elongated morphology of the radio PWN results from compression of the pulsar wind nebula by the SNR reverse shock.

This study demonstrates that a variety of useful constraints on the properties of an unseen central neutron star can be inferred from those of its associated PWN and SNR, provided that reasonable estimates for the system’s distance and age are available. With many new multiwavelength studies of PWN and composite SNRs now emerging, such an approach can be applied to many other sources.

We thank Bob Sault for allowing us to carry out the ATCA observations remotely from Harvard University, Dick Manchester for advance information on his pulsar survey of the LMC, Paul Plucinsky for help in planning of the *Chandra* observations, and Eric van der Swaluw and Patrick Slane for useful discussions. The Australia Telescope is funded by the Commonwealth of Australia for operation as a National Facility managed by CSIRO. This work was supported by NASA through SAO grant GO1-2075X and LTSA grant NAG5-13032.

REFERENCES

- Blondin, J. M., Chevalier, R. A., & Frierson, D. M. 2001, *ApJ*, 563, 806.
- Camilo, F., Kaspi, V. M., Lyne, A. G., Manchester, R. N., Bell, J. F., D’Amico, N., McKay, N. P. F., & Crawford, F. 2000, *ApJ*, 541, 367.
- Chevalier, R. A. 1998, *Mem. della Soc. Ast. It.*, 69, 977.
- Cusumano, G., Massaro, E., & Mineo, T. 2003, *A&A*, 402, 647.
- Frail, D. A., Giacani, E. B., Goss, W. M., & Dubner, G. 1996, *ApJ*, 464, L165.
- Gaensler, B. M., Pivovaroff, M. J., & Garmire, G. P. 2001, *ApJ*, 556, L107.
- Gotthelf, E. V., Vasish, G., Boylan-Kolchin, M., & Torii, K. 2000, *ApJ*, 542, L37. PSR J1846-0258.
- Helfand, D. J. & Becker, R. H. 1987, *ApJ*, 314, 203.
- Helfand, D. J., Gotthelf, E. V., & Halpern, J. P. 2001, *ApJ*, 556, 380.
- Hendrick, S. P. et al. 2003, in preparation.
- Hughes, J. P., Slane, P. O., Park, S., Roming, P. W. A., & Burrows, D. N. 2003, *ApJ*, in press (astro-ph/0305383).

PULSAR WIND NEBULA IN THE LMC

Kaspi, V. M. & Helfand, D. J. 2002, in *Neutron Stars in Supernova Remnants*, ed. P. O. Slane & B. M. Gaensler, (San Francisco: Astronomical Society of the Pacific), 3.

Katz-Stone, D. M. & Rudnick, L. 1997, *ApJ*, 488, 146.

Kramer, M. et al. 2003, *MNRAS*, in press (astro-ph/0303473).

Manchester, R. N., Fan, G., Lyne, A. G., Kaspi, V. M., & Crawford, F. 2003, in preparation.

Manchester, R. N., Staveley-Smith, L., & Kesteven, M. J. 1993, *ApJ*, 411, 756.

Manchester, R. N. & Taylor, J. H. 1977, *Pulsars*, (San Francisco: Freeman).

Murray, S. S., Slane, P. O., Seward, F. D., Ransom, S. M., & Gaensler, B. M. 2002, *ApJ*, 568, 226.

Pavlov, G. G., Zavlin, V. E., Sanwal, D., & Trümper, J. 2002, *ApJ*, 569, L95.

Porquet, D., Decourchelle, A., & Warwick, R. S. 2003, *A&A*, 401, 197.

Possenti, A., Cerutti, R., Colpi, M., & Mereghetti, S. 2002, *A&A*, 387, 993.

van der Swaluw, E., Achterberg, A., & Gallant, Y. A. 1998, *Mem. della Soc. Ast. It.*, 69, 1017.

van der Swaluw, E., Achterberg, A., Gallant, Y. A., & Tóth, G. 2001, *A&A*, 380, 309.

Wang, Q. D., Gotthelf, E. V., Chu, Y.-H., & Dickel, J. R. 2001, *ApJ*, 559, 275.

Weiler, K. W. & Panagia, N. 1980, *A&A*, 90, 269.

TABLE 1
RADIO PROPERTIES OF SNR B0453–685.

Waveband (cm)	Resolution (arcsec)	Flux Density (mJy)		
		Core	Shell	Total
1.4 GHz	7.3×6.7	46 ± 2	140 ± 2	186 ± 3
2.4 GHz	9.2×8.4	46 ± 2	105 ± 2	151 ± 3

TABLE 2
COMPARISON OF SNR B0453–685 TO OTHER SIMILAR SYSTEMS.

SNR	Distance (kpc)	Age (10^3 yr)	R_{SNR}	R_{PWN} (pc)	$L_{R,PWN}$	$L_{X,PWN}$ (10^{34} ergs s^{-1})	$L_{X,PSR}$	Ref ^b
B0453–685	50	13	29 ± 1	7×5	2	6	< 0.5	This paper
Vela SNR	0.3	~ 11	42	10	0.8	0.8 ^a	0.01	1, 2
G0.9+0.1	~ 10	$\sim 10 - 20$	20	6	7	6	0.06	3, 4

R_{SNR} and R_{PWN} are the radii of the SNR and PWN respectively; $L_{R,PWN}$ and $L_{X,PWN}$ are the approximate radio and X-ray luminosities, respectively, of the PWN. $L_{X,PSR}$ is the approximate X-ray luminosity of the central pulsar.

^aThe PWN luminosity quoted by Helfand et al. (2001) is much lower than this, but corresponds to only the innermost component of the PWN.

^bREFERENCES: (1) Weiler & Panagia (1980); (2) Helfand et al. (2001); (3) Helfand & Becker (1987); (4) Porquet et al. (2003).

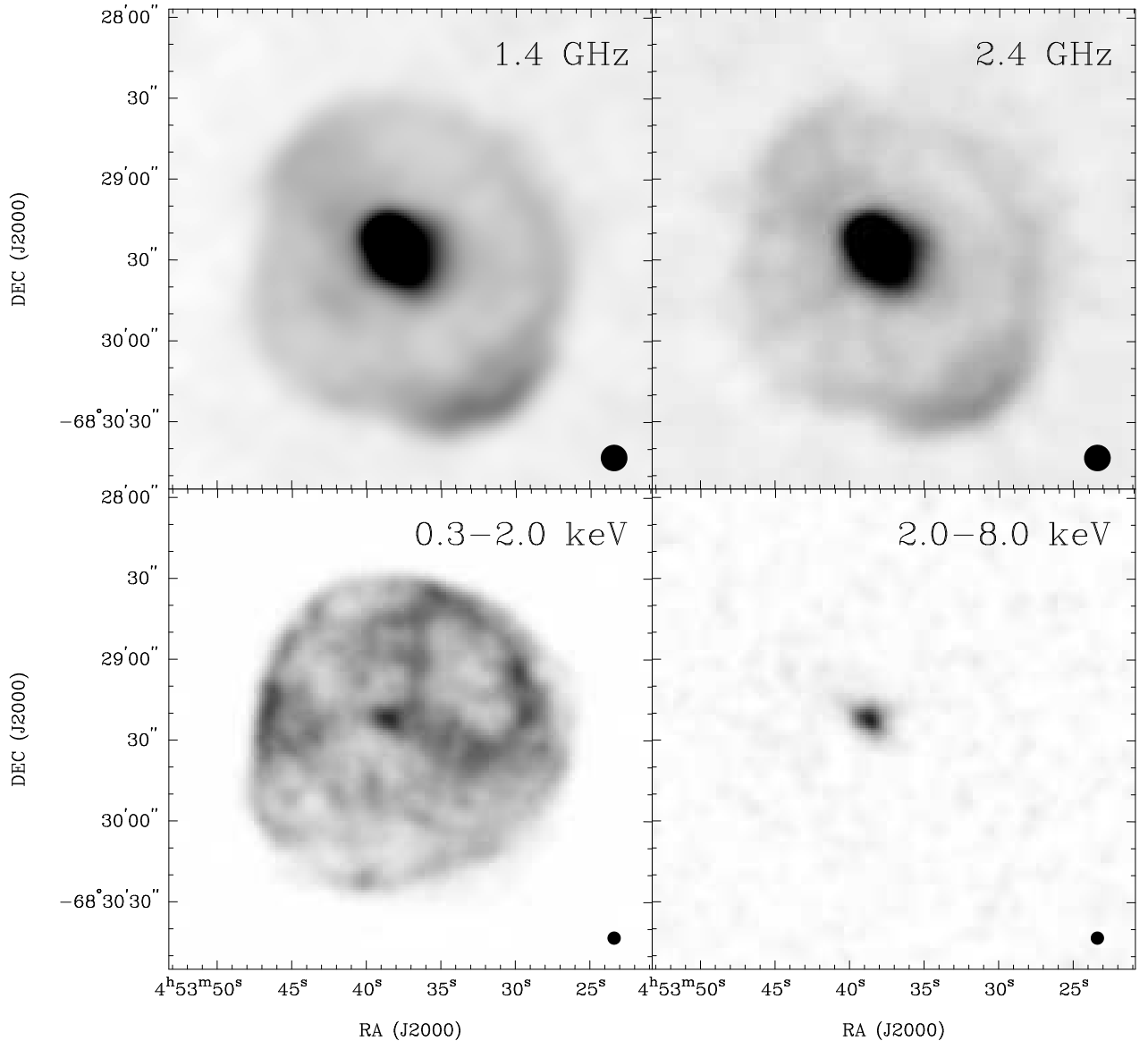


FIG. 1.— Radio and X-ray images of SNR B0453–685. The top two panels show ATCA radio images of the source at frequencies of 1.4 and 2.4 GHz, while the bottom two panels show *Chandra* X-ray images of B0453–685 in the soft and hard parts of the bandpass. The two radio images have both been smoothed to a resolution of $10'' \times 10''$. The sensitivity of the radio images are 95 and $65 \mu\text{Jy beam}^{-1}$ at 1.4 and 2.4 GHz respectively. Both radio images are shown over the same greyscale range, -0.4 to $+5.7 \text{ mJy beam}^{-1}$. The X-ray images have both been smoothed with a gaussian of FWHM $5'' \times 5''$. In all four panels, the dimensions of the resultant point-spread function are shown by the ellipse in the lower-right corner of the panel, and the greyscale is shown using a linear transfer function.

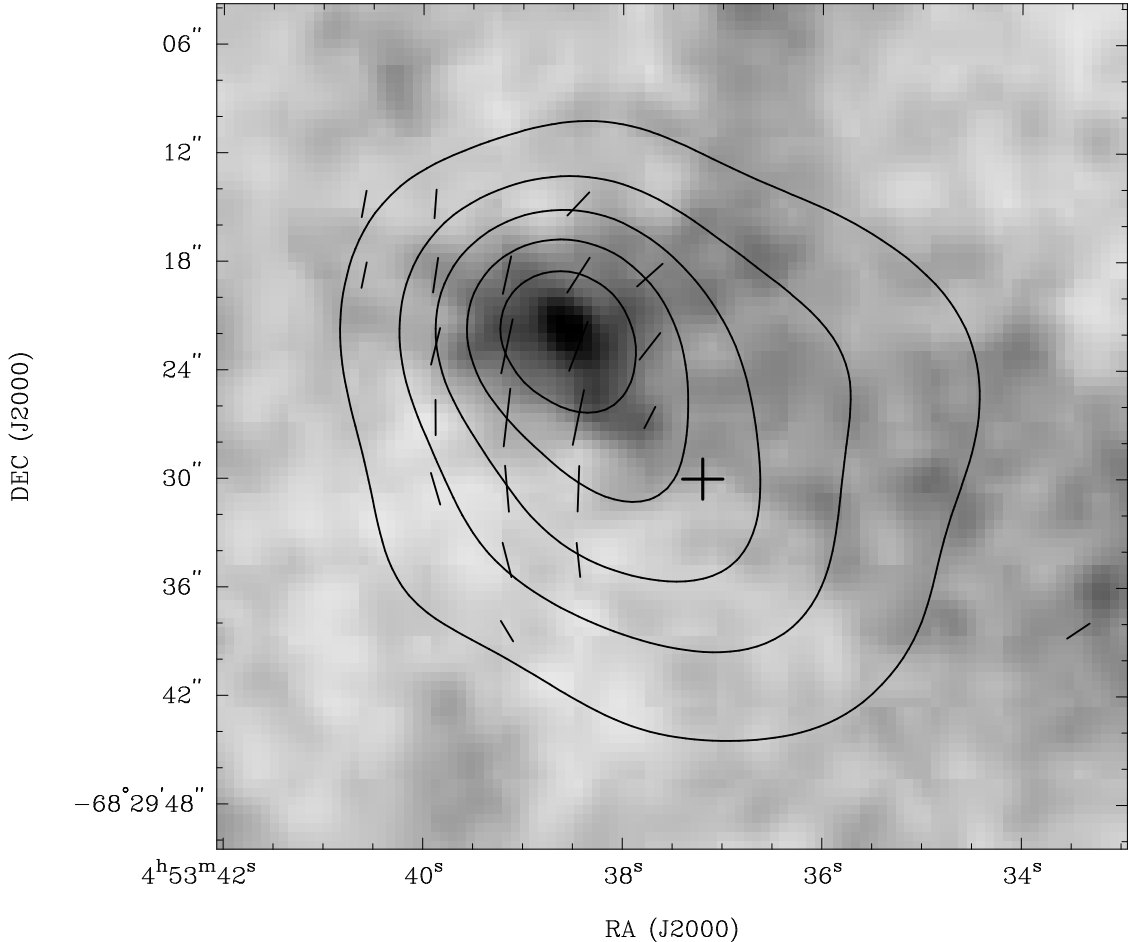


FIG. 2.—Radio and X-ray images of the core of SNR B0453–685. The greyscale shows X-ray emission from the central region of B0453–685 as seen by *Chandra* in the energy range 0.3–8.0 keV, smoothed to a resolution of $2''$. The contours represent the 2.4-GHz image at full resolution ($9.2'' \times 8.4''$), drawn at the levels of 2, 4, 6, 8 and 10 mJy beam $^{-1}$. Overlaid as vectors are the 2.4-GHz linearly polarized intensity at each position; the length of each vector is proportional to the polarized intensity (up to a maximum of 0.7 mJy beam $^{-1}$) and the orientation of the vector indicates the mean position angle of the electric field (averaged across the observing bandwidth, and not corrected for Faraday rotation). The “+” symbol indicates the center fitted for the surrounding SNR shell.